



Cite this: *RSC Adv.*, 2022, 12, 4446

# *In situ* integration of cobalt diselenide nanoparticles on CNTs realizing durable hydrogen evolution†

Hongfeng Ye, Xuejiao Zhou, Zhitao Shao, Jing Yao, Wenjie Ma, Lili Wu \* and Xinzhi Ma\*

Cobalt diselenide (CoSe<sub>2</sub>) is considered to be a promising economical and efficient electrocatalyst for the hydrogen evolution reaction (HER). Here carbon nanotubes (CNTs) were employed as a conductive skeleton to optimize the electrocatalytic performance of CoSe<sub>2</sub> through a simple one-step hydrothermal method. Beyond the expected, the introduction of CNTs not only accelerates electron transportation and ion diffusion, but also improves the reaction kinetics for HER by forming a CoSe<sub>2</sub>/CNT heterointerface. Consequently, the CoSe<sub>2</sub>/CNTs composite exhibits an optimal overpotential of 153 mV with a weight ratio of 10 : 1, and sustains a long period of 48 hours with a negligible overpotential deterioration. In addition, a Faraday efficiency of 97.67% is achieved with a H<sub>2</sub>/O<sub>2</sub> molar ratio of 2 : 1. Therefore, these results open up further opportunities for yielding efficient and durable hydrogen evolving electrocatalysts from low-cost transition metal compounds.

Received 30th September 2021

Accepted 22nd December 2021

DOI: 10.1039/d1ra07301j

rsc.li/rsc-advances

## 1 Introduction

With the serious consumption of fossil energy and concomitant environmental pollution, renewable energy is receiving increasing attention. Hydrogen is considered to be an effective solution for global energy shortage due to its advantages: high energy density, cleanliness, and renewability.<sup>1–3</sup> The electrolysis of water is an efficient way to produce hydrogen, and the most efficient cathode electrocatalysts toward the hydrogen evolution reaction (HER) are platinum-based catalysts, which have low overpotential and fast catalytic reaction kinetics. However, the high cost of platinum-based cathode electrocatalysts severely limits their large-scale commercial application.<sup>4,5</sup>

For saving costs, Pt or other noble metal-based electrocatalysts on atomic-level, like the noble-metal single-atom catalysts supported by non-noble substrate, have been extensively investigated.<sup>6,7</sup> Alternatively, non-noble-metal-based nanocatalysts including alloys, chalcogenides, phosphides, carbides and nitrides are closely pursued to maximize economic benefit.<sup>5,8–10</sup> Among these non-noble-metal-based nanocatalysts, transition metal selenides stand out from the crowd due to their more superior free energy than pristine metals for proton adsorption and relatively lower electrical conductivity than the

counterparts of sulfides.<sup>11</sup> Especially, CoSe<sub>2</sub> has received much attention due to its good electrical conductivity, good catalytic activity, huge storage on earth, and indispensability for human being.<sup>12–15</sup> Unfortunately, during the growth process, CoSe<sub>2</sub> commonly possesses a large individual size or tends to aggregate together, limiting the exposure of HER active center. In this regard, researchers devoted a lot of attentions aiming to enlarge the number of active centers of CoSe<sub>2</sub>. For example, Kim *et al.* integrated CoSe<sub>2</sub> with CNTs through a spray pyrolysis followed with a selenization.<sup>16</sup> The obtained CoSe<sub>2</sub>-CNTs composite has a porous structure, which increases the number of the exposed active centers besides guaranteeing fast ions' transmission in electrolyte. These advantages contributed CoSe<sub>2</sub>-CNTs an improved overpotential of 174 mV and a good long-term stability for 1000 cycles. Besides that, Yang *et al.* synthesized hollow mesoporous carbon (HC) nanospheres, wherein the carbon walls were grafted with CoSe<sub>2</sub> by successive infiltration and selenization processes.<sup>13</sup> The classical structure of HC not only facilitates the penetration of electrolyte and the exposure of active centers, but also stabilizes the structure by hindering electrolyte etching. As a result, the CoSe<sub>2</sub>@HC composites harvest an optimal overpotential of 171.7 mV at 10 mA cm<sup>−2</sup> and a stable HER for 12 h.

Although these exciting breakthroughs in exposing more active centers of CoSe<sub>2</sub> have been achieved, there's plenty room for stability improvement. Generally, HER stability is tested by rapid CV cycling for one to several thousand cycles, or under static (potential/galvanic) mode for several hours to a few days. At the end of these endurance tests, the change in overpotential or the percentage degradation in activity is frequently reported as the stability marker, and an increase in overpotential by

Key Laboratory for Photonic and Electronic Bandgap Materials, Ministry of Education, School of Physics and Electronic Engineering, Harbin Normal University, Harbin, 150025, People's Republic of China. E-mail: wll790107@hotmail.com; maxz@hrbnu.edu.cn

† Electronic supplementary information (ESI) available. See DOI: 10.1039/d1ra07301j



~30 mV or activity degradation no more than 5% is accepted as a good catalyst.<sup>10</sup> Furthermore, faradaic efficiency is an importantly index reflecting the selectivity of an electrocatalyst, scilicet the utilization efficiency of applied energy. It is usually less than 100%. A low faradaic efficiency should ascribe to the presence of side reactions.

Herein, we *in situ* grew CoSe<sub>2</sub> nanoparticles on CNTs *via* an artful one-pot hydrothermal method. The employment of CNTs guarantees fast ion and electronic transfer. In addition, it significantly restricts the growth and inhibits the agglomeration of CoSe<sub>2</sub> crystals. These advantages endow the CoSe<sub>2</sub>/CNTs composites obviously enlarged number of active centers, which is seriously conducive to HER activity. As a result, the CoSe<sub>2</sub>/CNTs composites output a current density of 10 mA cm<sup>-2</sup> with an optimal overpotential of 153 mV. More importantly, the CoSe<sub>2</sub>/CNTs composites exhibit an excellent stability in the long-term cycle test for 48 h, which is much superior to the commercial platinum carbon (Pt/C) composite electrode. The faradaic efficiency yielded during HER process is 97.67%.

## 2 Experimental sections

### 2.1 Materials

Carbon nanotube dispersion (TNWDM-M2) was purchased from Chinese Academy of Science, Chengdu Organic Chemistry Co. Ltd, NaBH<sub>4</sub> (CAS No: 16940-66-2, 98%), CoCl<sub>2</sub>·6H<sub>2</sub>O (CAS No: 7791-13-1, 98%), and Se (CAS No: 7782-49-2, 99.9%) powders were purchased from Aladdin Co. Ltd. All the chemicals are analytical grade without further purification.

### 2.2 Synthesis of CoSe<sub>2</sub>/CNTs composites

Firstly, 671 μL carbon nanotube solution (41.2 mg mL<sup>-1</sup>) was added into 20 mL deionized (DI) water, and then ultrasound for one hour to make it dispersed evenly. Secondly, 215 mg Se powder and 128.6 mg NaBH<sub>4</sub> were dissolved in 10 mL DI, and named it as solution A after being dispersed evenly. Thirdly, the dispersed carbon nanotube solution and 323.18 mg CoCl<sub>2</sub>·6H<sub>2</sub>O were added into solution A and then dispersed evenly. Finally, the prepared solution was transferred to a 50 mL Teflon-lined autoclave, and then it was heated at 200 °C for 20 hours. The product obtained after the hydrothermal treatment was washed with DI, and then vacuum dried at 60 °C. Except for adding CNTs, the synthesis method of pure CoSe<sub>2</sub> is the same as that of CoSe<sub>2</sub>/CNTs.

### 2.3 Preparation of CoSe<sub>2</sub>/CNTs electrodes

Weigh 20 mg CoSe<sub>2</sub>/CNTs and grind it in a mortar for 1–2 h. CoSe<sub>2</sub>/CNTs and 5 wt% polyvinylidene fluoride (PVDF) (mass ratio: CoSe<sub>2</sub>/CNTs : PVDF is 9 : 1) were added to NMP, ultrasonic treatment for 3 hours to obtain uniformly dispersed ink. The 1 mg/10 μL ink was evenly coated on hydrophilic carbon paper (1 cm × 1 cm, load ≈ 2 mg cm<sup>-2</sup>) by drip coating, and dried under vacuum at 60 °C for 12 hours.

For comparison, pure CoSe<sub>2</sub> nanoparticles without CNTs and the mixture of CoSe<sub>2</sub> nanoparticles with CNTs (denoted as CoSe<sub>2</sub>-CNTs) were also coated onto hydrophilic carbon paper to prepare pure CoSe<sub>2</sub> and CoSe<sub>2</sub>-CNTs electrodes using the same method.

### 2.4 Characterization

Scanning electron microscope (SEM, SU70, Hitachi, Japan) analyzes the morphology of the composite material. The microstructure of the material was further characterized by a transmission electron microscope (TEM, FEI, Tecnai TF20) with an energy dispersive X-ray spectrometer (EDX). Use X-ray diffraction (XRD, D/max 2600, Rigaku, Japan) with Cu Kα radiation (λ = 1.5418 Å) to characterize the crystal structure of the material. The Raman spectrum was measured with a miniature Raman spectrometer (JY; HR800, France) at an excitation wavelength of 488 nm. The chemical composition of the material was characterized by X-ray photoelectron spectroscopy (XPS, Thermo ESCALAB 250Xi).

### 2.5 Electrochemical measurements

The composite material's electrochemical catalytic ability, stability and other electrochemical properties were tested by the VMP3 electrochemical workstation (France Bio-logic) in three-electrode configuration. The pre-prepared electrode was used as the working electrode, the saturated calomel electrode (SCE) was used as the reference electrode, and the carbon rod was used as the counter electrode.

The polarization curve was obtained by linear sweep voltammetry (LSV) at 5 mV s<sup>-1</sup>. Electrochemical impedance spectroscopy (EIS) was tested under an overpotential of -0.25 V (vs. RHE), and the frequency parameter was 100 mHz to 100 kHz. Cyclic voltammetry (CV) was used to measure the electric double-layer capacitance (C<sub>dl</sub>) at 0.45–0.55 V (vs. RHE) and the scan rate range was 20–200 mV. Turnover frequency (TOF) was obtained from the CV test in a pH = 7 phosphate buffer (PBS), within the voltage range of -0.2–0.6 V (vs. RHE), the scan rate was 50 mV s<sup>-1</sup>. The scanning rate was 100 mV s<sup>-1</sup> for 3000 CV tests, and the chronopotentiometry was used for a 48 h long cycle test at 30 mA cm<sup>-2</sup> to investigate the catalytic stability of

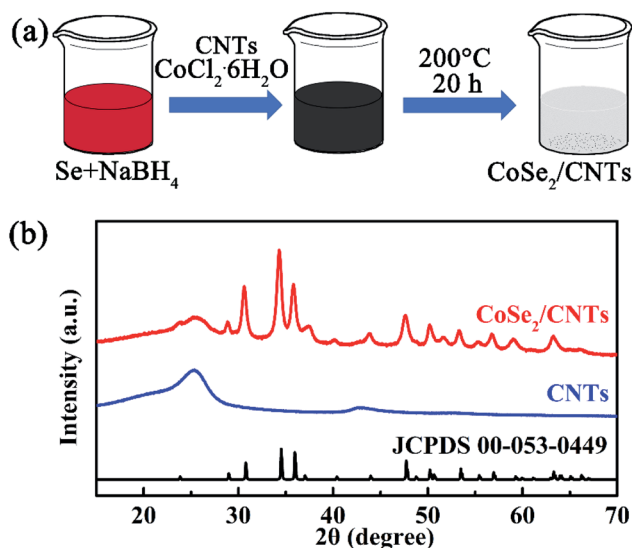


Fig. 1 (a) Preparation process of CoSe<sub>2</sub>/CNTs composite, and (b) XRD patterns of CoSe<sub>2</sub>/CNTs composite and CNTs.

the catalyst. All overpotentials were corrected by 85% ohm potential drop ( $iR$ ) compensation.

### 3 Results and discussion

#### 3.1 Morphologies and structures

Fig. 1a illustrates the facile preparation process of  $\text{CoSe}_2/\text{CNTs}$  composites. First, Se and  $\text{NaBH}_4$  powders were added into deionized water and stirred continuously. When the aqueous solutions were homogeneous, the pre-dispersed CNTs suspension with a certain amount of  $\text{CoCl}_2 \cdot 6\text{H}_2\text{O}$  dissolved in it was added. The CNTs here used are multiwall CNTs with a uniform diameter of  $\sim 10$  nm (Fig. S1†). After the hydrothermal treatment at  $200^\circ\text{C}$  for 20 hours, final products were obtained. In

order to analyze their crystalline structure, XRD test was first conducted. As shown in Fig. 1b, the wide peak located at  $\sim 26^\circ$  belongs to CNTs, and other diffraction peaks all derive from the orthorhombic structure of  $\text{CoSe}_2$  (JCPDS #00-053-0449).<sup>17</sup> It strongly confirmed that orthorhombic  $\text{CoSe}_2$  nanocrystallines have been grown *in situ* on the surface of CNTs (denoted as  $\text{CoSe}_2/\text{CNTs}$ ) with no impurities observed.

The morphology of the  $\text{CoSe}_2/\text{CNTs}$  composite is characterized by SEM. In Fig. 2a, numerous nanoparticles can be clearly watched snatchily decorating the surface of CNTs without severely agglomeration. The size of these nanoparticles mainly ranges from 10 nm to 30 nm, and the average diameter of  $\sim 100$  nanoparticles is 22.5 nm (the inset in Fig. 2a). It is remarkably smaller than that of the bare  $\text{CoSe}_2$  nanoparticles (37.5 nm)

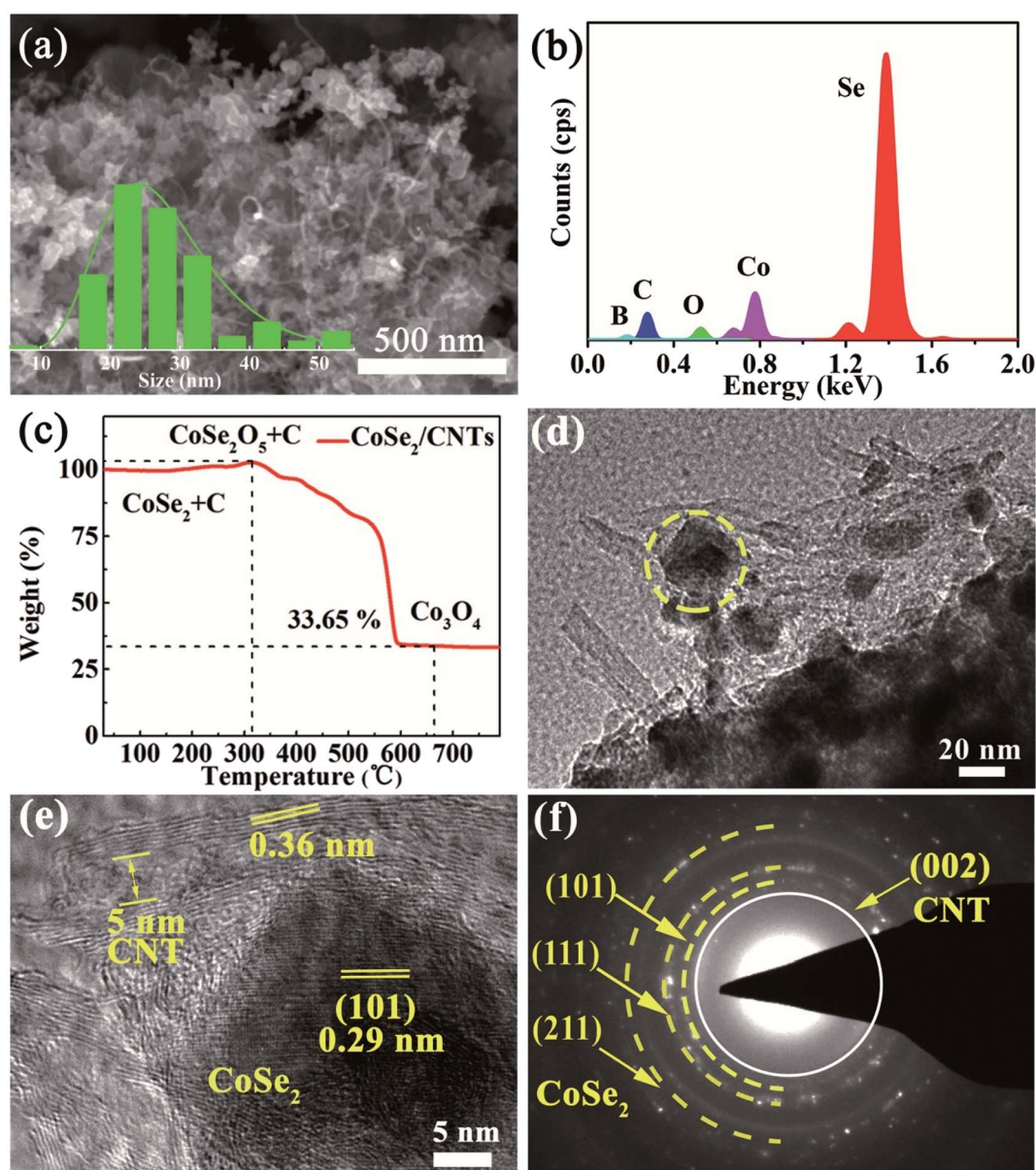


Fig. 2 (a) SEM image, inset shows grain size distribution of  $\text{CoSe}_2$  nanoparticles, (b) EDS spectrum, (c) TGA curves image, (d) TEM image, and (e) HRTEM image, and (f) SAED pattern of  $\text{CoSe}_2/\text{CNTs}$  composite.





preparing under the same conditions (Fig. S2 and S3†). Meanwhile, the smaller nanoparticles in the composite exhibit better distribution than bare  $\text{CoSe}_2$  nanoparticles, which is desirable for high-performance HER electrocatalysis. In Fig. 2b, EDX analysis reveals that the composite consists of Se, Co, C, B, and O elements. The stoichiometric ratio of Co and Se is nearly 1 : 2, indicating the small nanoparticles in the composite are  $\text{CoSe}_2$  nanoparticles. B element should be inherited from sodium borohydride precursor and conducive for HER. O element might be due to the partial oxidation of  $\text{CoSe}_2$  (*vide infra*).

The weight ratio of  $\text{CoSe}_2$  and CNTs was subsequently investigated by thermogravimetric analysis (TGA). As shown in

Fig. 2c, the slight weight loss before 200 °C is derived from the evaporation of adsorbed water in the sample, and the slight increase in weight between 200–350 °C is related to the oxidation of  $\text{CoSe}_2$ . The weight loss between 350–800 °C is due to the further conversion from  $\text{CoSe}_2\text{O}_5$  to  $\text{Co}_3\text{O}_4$  along with the combustion of CNTs.<sup>18</sup> Finally, according to the  $\text{Co}_3\text{O}_4$  content displayed by the TGA curve, the  $\text{CoSe}_2$  content in  $\text{CoSe}_2/\text{CNTs}$  is calculated to be 90.89 wt%. That is, the  $\text{CoSe}_2$  : CNTs weight ratio approaches to 10 : 1. Fig. 2d is a typical TEM image of the  $\text{CoSe}_2/\text{CNTs}$  composite, in which it shows the irregular morphology and nonuniform diameters of the  $\text{CoSe}_2$  nanoparticles in composite. In Fig. 2e (corresponding to the yellow

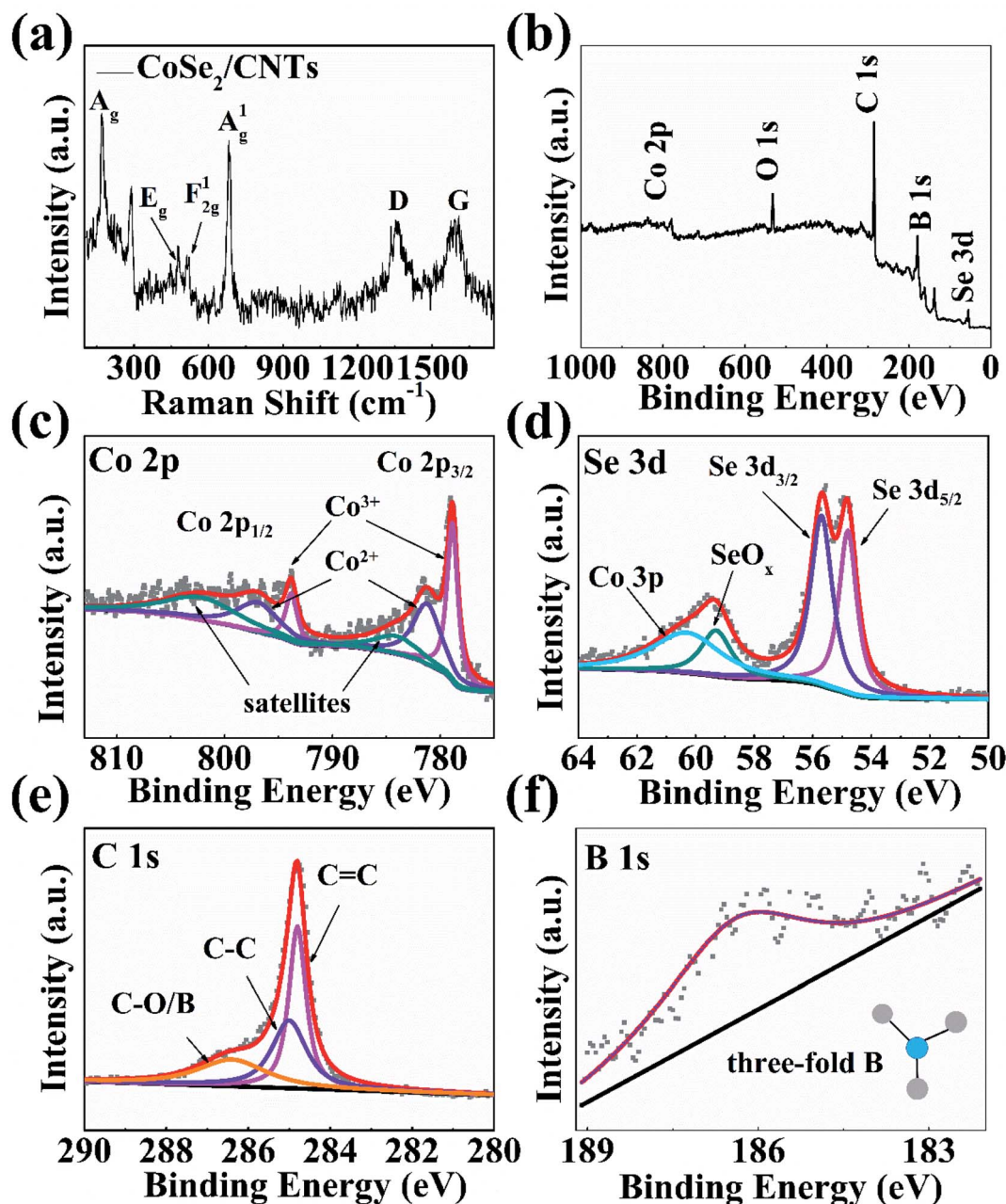


Fig. 3 (a) Raman image, (b) XPS survey spectrum, (c) Co 2p, (d) Se 3d and (e) C 1s and (f) B 1s XPS spectra of  $\text{CoSe}_2/\text{CNT}$  composite.

dashed area in Fig. 2d), well-resolved lattice fringes of 0.29 nm are corresponding to the (101) crystal plane of CoSe<sub>2</sub>, and the ones of 0.36 nm belong to the (002) plane of CNTs. The wall number of CNTs is 5–10, and the inner diameter is ~5 nm. Fig. 2f is the SAED pattern of CoSe<sub>2</sub>/CNTs composite. It mainly exhibits four concentric rings. The three yellow lines marked ones are indexed to the (101), (111), and (211) of orthorhombic CoSe<sub>2</sub>, and the white one corresponds to the (002) crystal plane of CNTs,<sup>19</sup> confirming the successful construction of CoSe<sub>2</sub>/CNTs composite with both polycrystalline nature of CoSe<sub>2</sub> nanoparticles and CNTs.<sup>20</sup>

More structural features of the CoSe<sub>2</sub>/CNTs composite were further revealed by the Raman spectrum. In Fig. 3a, the two sharp peaks located at 173.5 and 674 cm<sup>-1</sup> are the fingerprint characters of orthorhombic CoSe<sub>2</sub> and correspond to the A<sub>g</sub> and A<sub>1g</sub> modes, and other two tiny ones at 469, 512 cm<sup>-1</sup> correspond to the E<sub>g</sub> and F<sub>2g</sub> modes of orthorhombic CoSe<sub>2</sub>. Besides, the peaks appearing at 1354 and 1584 cm<sup>-1</sup> are corresponded to the sp<sup>3</sup> (D band) and sp<sup>2</sup> (G band) hybridizations of carbonaceous materials, respectively.<sup>21</sup> The intensity ratio (*I*<sub>D</sub>/*I*<sub>G</sub>) is often used as a diagnostic tool for evaluating the disordered degree of carbonaceous materials. Here it is calculated to be 1.02, implying the existence of affluent carbon defects. The local electronic structures of the CoSe<sub>2</sub>/CNTs composite were elucidated by XPS measurement. The XPS survey spectrum confirms Co, Se, C, B, and O elements in the composite (Fig. 3b). The Co 2p spectrum in Fig. 3c presents two broad peaks of Co 2p<sub>3/2</sub>

(781.2 eV) and Co 2p<sub>1/2</sub> (796.9 eV) consisting of three doublets: Co<sup>2+</sup> (Co–Se), Co<sup>3+</sup> (Co–O/B, arising from the partial surface oxidation of CoSe<sub>2</sub>),<sup>22</sup> and satellite peaks. In Fig. 3d, the Se 3d spectrum consists of pronounced Se 3d<sub>3/2</sub>, Se 3d<sub>5/2</sub> and SeO<sub>x</sub> (the partial oxidation of CoSe<sub>2</sub>).<sup>23</sup> The C 1s signal (Fig. 3e) mainly contains C=C, C–C, and C–O/B bonds.<sup>16</sup> Fig. 3f shows the XPS high-resolution spectrum of the B 1s region. The B 1s signal is located at 186.5 eV, which belongs to the three-fold coordination of B element.<sup>24,25</sup> It is reasonable to believe that the presence of three fold coordinated B element would increase defect density and improve the HER performance of CoSe<sub>2</sub>/CNTs composite.

### 3.2 Electrochemical performances

The CoSe<sub>2</sub>/CNTs composite was measured electrochemical performances in 0.5 M H<sub>2</sub>SO<sub>4</sub>. For comparison, commercial Pt/C (20%), pure CoSe<sub>2</sub> and CNTs were also checked. In Fig. 4a, the CoSe<sub>2</sub>/CNTs composite only needs 153 mV overpotential to achieve 10 mA cm<sup>-2</sup>. Based on the phenomenon that CNTs has almost no HER performance, the catalytic performance of CoSe<sub>2</sub>/CNTs composite could be completely attributed to CoSe<sub>2</sub> nanoparticles. While compared with the overpotential of 189 mV for bare CoSe<sub>2</sub> nanoparticles, the overpotential differential of 36 mV should profit from the introduction of CNTs supporting. Furthermore, the compact connections of CNTs with CoSe<sub>2</sub> nanoparticles derived from the *in situ* growth also

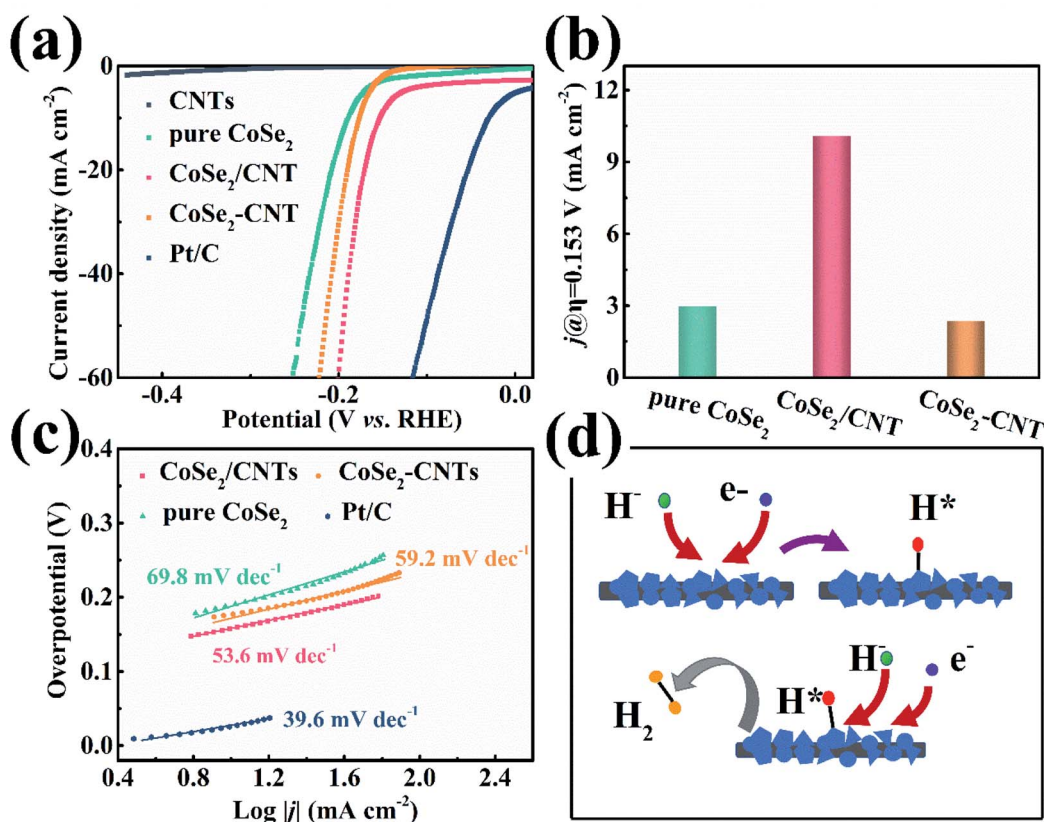


Fig. 4 (a) Polarization curve, (b) cathode current density at the same voltage (c) Tafel slope, and (d) reaction mechanism diagram.



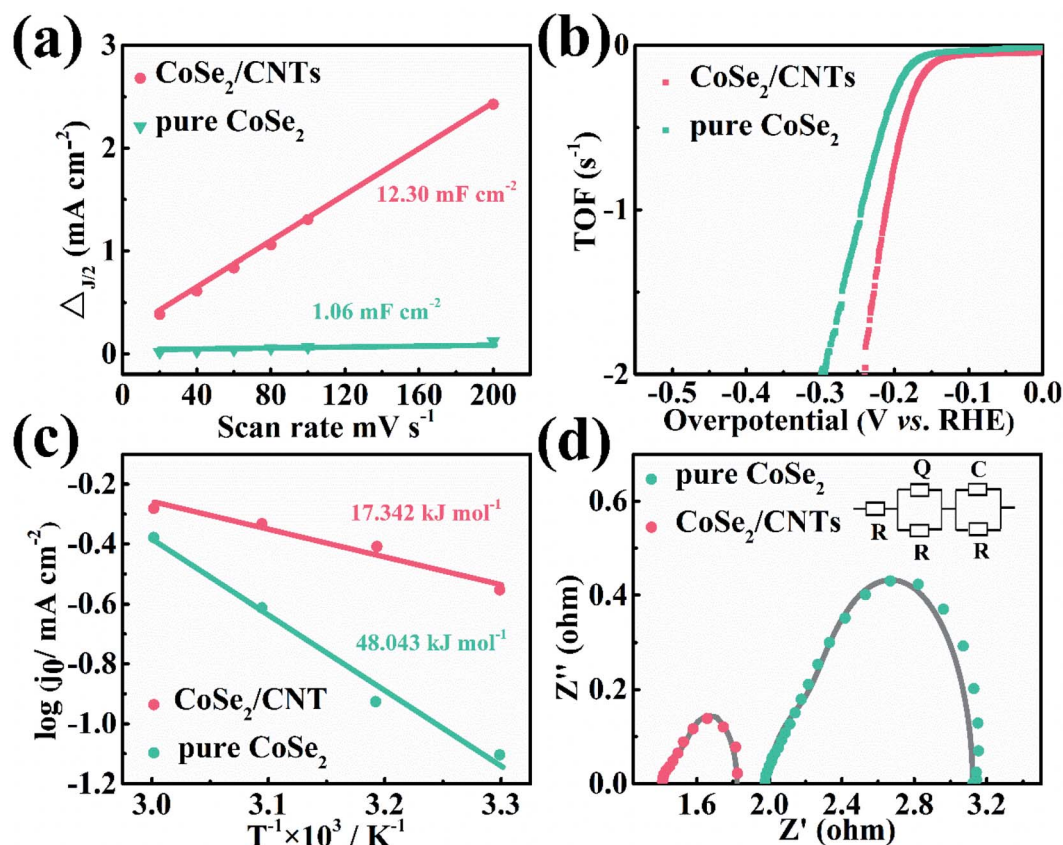


Fig. 5 (a)  $C_{dl}$  value of different electrodes, (b) TOF data measured in PBS solution, (c) Arrhenius plots for the tested electrode materials and (d) electrochemical impedance spectra, inset shows the equivalent circuit (the gray line is the fitted curve of the equivalent circuit diagram).

plays a vital role in boosting the catalytic activity of CoSe<sub>2</sub> for HER, which can be validated by the further comparison with the mixture of bare CoSe<sub>2</sub> nanoparticle and CNTs (denoted as CoSe<sub>2</sub>-CNTs). The CoSe<sub>2</sub>-CNTs needs 177 mV overpotential to achieve 10 mA cm<sup>-2</sup>, which is still 24 mV higher than CoSe<sub>2</sub>/CNTs composite. It should be noted that the CNTs content in CoSe<sub>2</sub>/CNTs composite has a significant impact on the electrocatalytic property of resultant composite (Fig. S4†). As CNTs content increases, the overpotential (10 mA cm<sup>-2</sup>) of CoSe<sub>2</sub>/CNTs composites firstly ameliorates from 189 mV and then deteriorates to 173 mV. The optimal overpotential of 153 mV is obtained from the CoSe<sub>2</sub>/CNTs composite with a weight ratio of CoSe<sub>2</sub> : CNTs = 10 : 1. To directly illustrate the superiority of CoSe<sub>2</sub>/CNTs composite to the bare CoSe<sub>2</sub> nanoparticles and CoSe<sub>2</sub>-CNTs in catalytic activity, the current density at the fixed overpotential of 0.153 V (vs. RHE) are recorded (Fig. 4b). The current density of 10 mA cm<sup>-2</sup> for the CoSe<sub>2</sub>/CNTs composite is 3.35 and 4.23 times of pure CoSe<sub>2</sub> (2.98 mA cm<sup>-2</sup>) and times of CoSe<sub>2</sub>-CNTs (2.36 mA cm<sup>-2</sup>), respectively. The Tafel slope values of these catalysts can be obtained from Fig. 4c. Obviously, CoSe<sub>2</sub>/CNTs composite has the smallest Tafel slope value of 53.6 mV dec<sup>-1</sup>, which is smaller than both of bare CoSe<sub>2</sub> (69.8 mV dec<sup>-1</sup>) and CoSe<sub>2</sub>-CNTs (59.2 mV dec<sup>-1</sup>), indicating the introduction of conductive CNTs scaffold and the formation of CoSe<sub>2</sub>/CNT heterointerface have obviously accelerated the

reaction kinetics. According to the Tafel equation,<sup>26,27</sup> the charge transfer coefficient of the CoSe<sub>2</sub>/CNTs composite is 1. The rate-determining step (RDS) involves zero electron transfer, and the number of electron transfer before RDS is 1. It means the RDS of the HER process of the CoSe<sub>2</sub>/CNTs composite is the Tafel reaction. Based on the above analysis, the reaction mechanism of the CoSe<sub>2</sub>/CNTs composite is deduced as shown in Fig. 4d. Firstly, the active site on the surface of CoSe<sub>2</sub>/CNTs composite capture a hydrogen ion (H<sup>+</sup>) and an electron to form an adsorbed hydrogen atom (H\*). Then, the subsequently generated H\* recombined with the adjacent H\* to evolve H<sub>2</sub>. Thus, the obviously accelerated reaction kinetics of CoSe<sub>2</sub>/CNTs composite than bare CoSe<sub>2</sub> and CoSe<sub>2</sub>-CNTs should attribute to the speed up generation of H\*.

The  $C_{dl}$  values of CoSe<sub>2</sub>/CNTs composite and bare CoSe<sub>2</sub> were estimated from the CV curves in Fig. S5.† The rectangular shape implies the favorable ion and electron transport of CoSe<sub>2</sub>/CNTs composite. In Fig. 5a, the linear slope, that is  $C_{dl}$  value, is 12.30 mF cm<sup>-2</sup> for the CoSe<sub>2</sub>/CNTs composite. It is significantly larger than that of bare CoSe<sub>2</sub> nanoparticles (1.06 mF cm<sup>-2</sup>), which should give the credit to the smaller size and better distribution of the CoSe<sub>2</sub> nanoparticles in the composite than bare CoSe<sub>2</sub> ones (Fig. 2a and S2†) besides the hollow structure of CNTs. The TOF value of CoSe<sub>2</sub>/CNTs composite can be extracted from the CV curve in Fig. S6.† According to the eqn (1):<sup>28</sup>



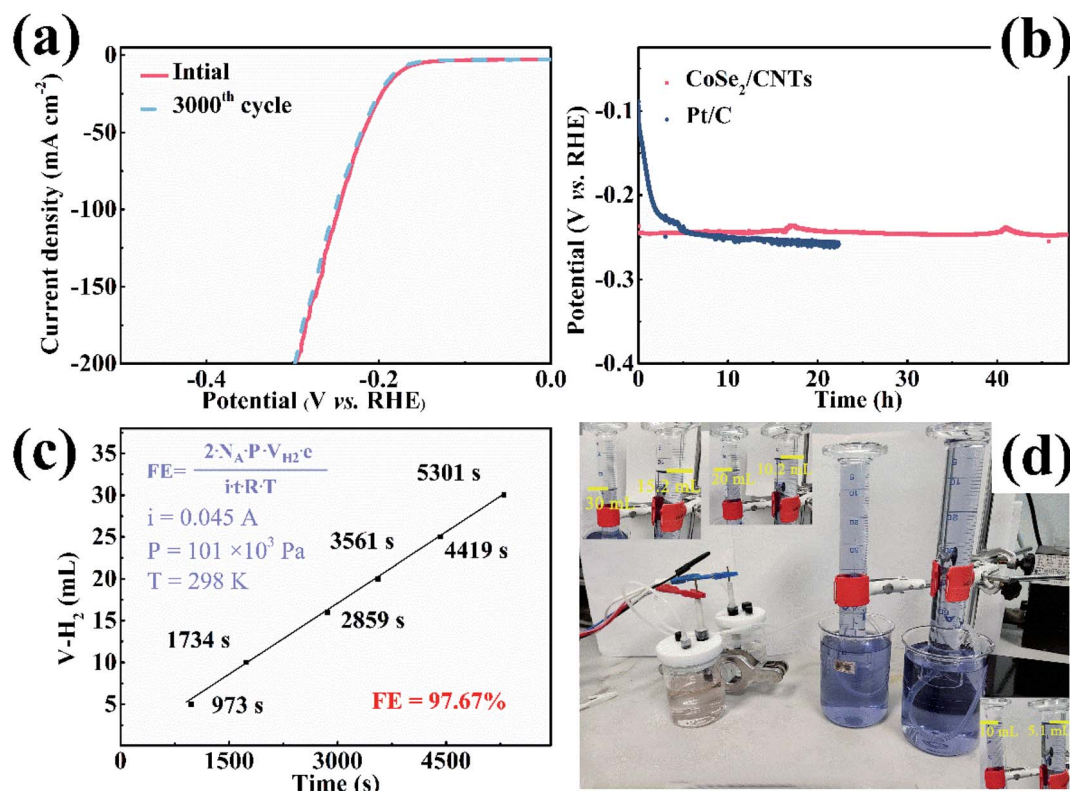


Fig. 6 (a) LSV data of CoSe<sub>2</sub>/CNTs before and after 3000 cycles, (b) long-term stability measurement of CoSe<sub>2</sub>/CNTs and Pt/C, (c) quantitative analysis of Faraday efficiency and (d) collecting H<sub>2</sub>/O<sub>2</sub> by water and gas displacement.

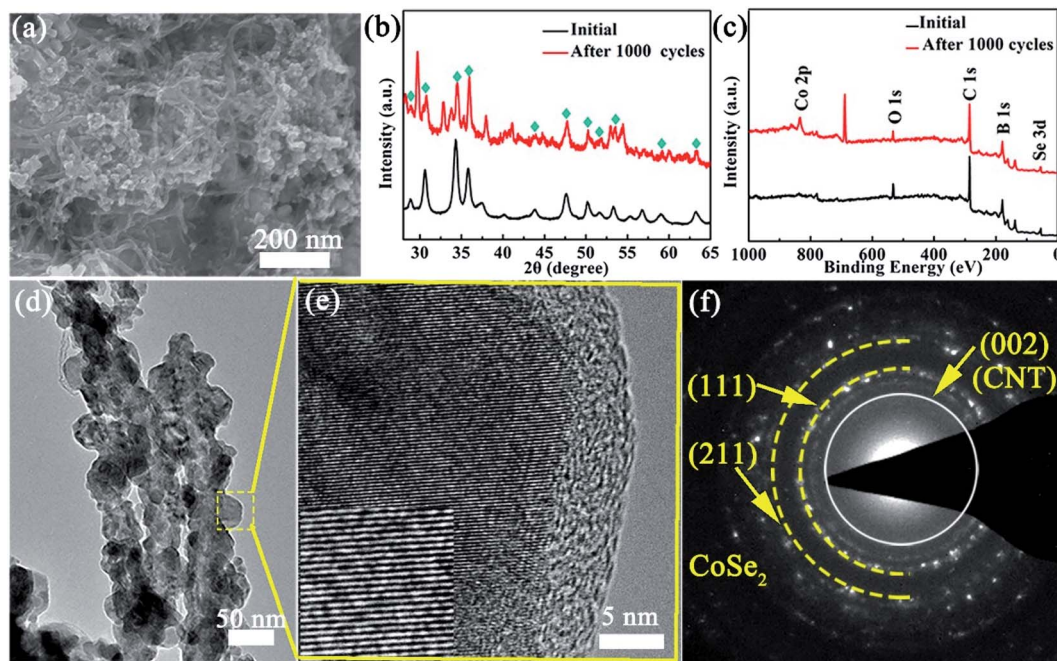


Fig. 7 (a) SEM image, (b) XRD image, (c) XPS survey spectrum, (d) TEM image, (e) HRTEM image, the inset is the enlarged HRTEM image, and (f) SAED pattern of CoSe<sub>2</sub>/CNT composite after cycling measurement.



$$\text{TOF (s}^{-1}\text{)} = (j \times A)/(2 \times n \times F) \quad (1)$$

where  $j$  is the current density,  $A$  is the test area,  $n$  is the number of active sites (mol), and  $F$  is the Faraday constant. As shown in Fig. 5b, CoSe<sub>2</sub>/CNTs composite only needs an overpotential of 189 mV to achieve a TOF of 0.5 s<sup>-1</sup>, while bare CoSe<sub>2</sub> nanoparticles need 216 mV. It reveals that the improved HER catalytic performance of CoSe<sub>2</sub>/CNTs composite is not only due to the large number of active sites, but also related to the boosted catalytic activity of each active site. A deeper understanding on the intrinsic activity of CoSe<sub>2</sub>/CNTs composite can be obtained from the LSV curves obtained at different temperatures (Fig. S7†). In Fig. 5c, the activation energy ( $E_a$ ) of CoSe<sub>2</sub>/CNTs composite is calculated to be 17.342 kJ mol<sup>-1</sup> according to the eqn S1,† which is only one third of that of bare CoSe<sub>2</sub> nanoparticles (48.043 kJ mol<sup>-1</sup>). The lower activation energy facilitates the reduction of H<sub>2</sub>O and enhancement of HER kinetics. The Nyquist plots in Fig. 5d are used to evaluate the charge transfer ability of CoSe<sub>2</sub>/CNTs composite. Employing the equivalent circuit in the inset of Fig. 5d, the fitting series resistance ( $R_s$ ), charge-transfer resistance ( $R_{ct}$ ), and mass transfer resistance ( $R_m$ ) of CoSe<sub>2</sub>/CNTs composite are 1.406, 0.163, and 0.253 Ω, respectively, indicating a fast electron transfer rate in the HER process of CoSe<sub>2</sub>/CNTs composite. More importantly, these three resistances are totally smaller than those of bare CoSe<sub>2</sub> (1.982, 0.320, and 0.82 Ω), which proves the enhancement of charge transfer ability arising from the incorporation of CNTs.

Durability is a significant indicator for the practical application of an electrocatalyst. In Fig. 6a, the LSV curve of CoSe<sub>2</sub>/CNTs composite after 3000 CV cycles superimposes over the initial curve before cycling with an ignorable increase of 6 mV in overpotential, indicating the excellent stability of CoSe<sub>2</sub>/CNTs composite. The chronopotentiometric curve of the CoSe<sub>2</sub>/CNTs composite was captured at 30 mA cm<sup>-2</sup> (Fig. 6b). It shows the deterioration of 5% in overpotential after a long period of 48 hours, which is obviously superior to the unstable catalytic performance of Pt/C. The calculated Faraday efficiency at a constant current of 45 mA of CoSe<sub>2</sub>/CNTs electrode is 97.67% with a H<sub>2</sub>/O<sub>2</sub> molar ratio of 2 : 1 (Fig. 6c and d). The CoSe<sub>2</sub>/CNTs composite after cycling was characterized by SEM, XRD, XPS, and TEM (Fig. 7 and S8†). In short, there is almost no change in morphology and microstructure after cycling. Especially, the well resolved lattice fringes without malposition in Fig. 7e and the sharp diffraction pattern in Fig. 7f provide reasonable assurance regarding the excellent stability of CoSe<sub>2</sub>/CNTs composite, which is remarkable compared with the reported CoSe<sub>2</sub>-based composite electrocatalysts (Table S1†). The high stability of CoSe<sub>2</sub>/CNTs composite should be attributed to the compact connections of CNTs with CoSe<sub>2</sub> nanoparticles derived from the *in situ* growth.

## 4 Conclusions

In summary, artful CoSe<sub>2</sub>/CNTs composites were synthesized by a simple one-step hydrothermal method. The optimal overpotential of CoSe<sub>2</sub>/CNTs composites is 153 mV. Furthermore,

the CoSe<sub>2</sub>/CNTs composite sustains a superior durability to commercial Pt/C electrode with Faraday efficiency nearly 100%. These desirable performances are attributed to the conductive CNTs scaffold, the smaller size and better distribution of the CoSe<sub>2</sub> nanoparticles, as well as the compact connections of CoSe<sub>2</sub> nanoparticles with CNTs. It is reasonable to believe these results open up further opportunities for yielding efficient and durable hydrogen evolving electrocatalysts from low-cost transition metal compounds.

## Author contributions

Hongfeng Ye, conceptualization, data curation, writing – original draft, Xuejiao Zhou, data curation, Zhitao Shao, data curation, Jing Yao, data curation, Wenjie Ma, data curation, Lili Wu, writing – review & editing and Xinzhi Ma writing – review & editing.

## Conflicts of interest

The authors declare no competing financial interest.

## Acknowledgements

This work was partially supported by the National Natural Science Foundation of China (No. 11504097, 51772069, 52072099), Team program of the Natural Science Foundation of Heilongjiang Province, China (No. TD2021E005).

## References

- 1 Z. P. Lin, B. B. XiaO, Z. P. Wang, W. Y. Tao, S. J. Shen, L. G. Huang, J. T. Zhang, F. Q. Meng, Q. H. Zhang, L. Gu and W. W. Zhong, *Adv. Funct. Mater.*, 2021, **31**, 2102321.
- 2 T. Egeland-Eriksen, A. Hajizadeh and S. Sartori, *Int. J. Hydrogen Energy*, 2021, **46**, 31963–31983.
- 3 M. Yue, H. Lambert, E. Pahon, R. Roche, S. Jemei and D. Hissel, *Renewable Sustainable Energy Rev.*, 2021, **146**, 111180.
- 4 N. Dubouis and A. Grimaud, *Chem. Sci.*, 2019, **10**, 9165–9181.
- 5 F. Zhou, Y. Zhou, G. G. Liu, C. T. Wang and J. Wang, *Rare Met.*, 2021, **40**, 3375–3405.
- 6 X. H. He, Y. C. Deng, Y. Zhang, Q. He, D. Q. Xiao, M. Peng, Y. Zhao, H. Zhang, R. C. Luo, T. Gan, H. B. Ji and D. Ma, *Cell Rep. Phys. Sci.*, 2020, **1**, 100004.
- 7 D. W. Ma, T. X. Li, Q. G. Wang, G. Yang, C. Z. He, B. Y. Ma and Z. S. Lu, *Carbon*, 2015, **95**, 756–765.
- 8 P. Yu, F. Wang, T. A. Shifa, X. Zhan, X. Lou, F. Xia and J. He, *Nano Energy*, 2019, **58**, 244–276.
- 9 D. Zhang, X. Hui, C. Y. Wu and Y. B. Zhu, *ChemCatChem*, 2021, **13**, 3370–3380.
- 10 J. Pan, S. W. Yu, Z. W. Jing, Q. T. Zhou, Y. F. Dong, X. D. Lou and F. Xia, *Small Struct.*, 2021, **2**, 2100076.
- 11 S. Anantharaj, S. Kundu and S. Noda, *J. Mater. Chem. A*, 2020, **8**, 4174–4192.
- 12 C. L. McCarthy, C. A. Downes, E. C. Schueller, K. Abuyen and R. L. Brutchey, *ACS Energy Lett.*, 2016, **1**, 607–611.





- 13 S. H. Yang, G. D. Park, J. K. Kim and Y. C. Kang, *Chem. Eng. J.*, 2021, **424**, 130341.
- 14 C. P. Lee, W. F. Chen, T. Billo, Y. G. Lin, F. Y. Fu, S. Samireddi, C. H. Lee, J. S. Hwang, K. H. Chen and L. C. Chen, *J. Mater. Chem. A*, 2016, **4**, 4553–4561.
- 15 K. Wang, D. Xi, C. J. Zhou, Z. Q. Shi, H. Y. Xia, G. W. Liu and G. J. Qiao, *J. Mater. Chem. A*, 2015, **3**, 9415–9420.
- 16 J. K. Kim, G. D. Park, J. H. Kim, S. K. Park and Y. C. Kang, *Small*, 2017, **13**, 1700068.
- 17 H. H. Yue, B. Yu, F. Qi, J. H. Zhou, X. Q. Wang, B. J. Zheng, W. L. Zhang, Y. R. Li and Y. F. Chen, *Electrochim. Acta*, 2017, **253**, 200–207.
- 18 J. Yang, H. C. Gao, S. Men, Z. Q. Shi, Z. Lin, X. W. Kang and S. W. Chen, *Adv. Sci.*, 2018, **5**, 1800763.
- 19 Z. T. Shao, L. L. Wu, Y. Yang, X. Z. Ma, L. Li, H. F. Ye and X. T. Zhang, *New Carbon Mater.*, 2021, **36**, 219–226.
- 20 H. X. Zhang, B. Yang, X. L. Wu, Z. J. Li, L. C. Lei and X. W. Zhang, *ACS Appl. Mater. Interfaces*, 2015, **7**, 1772–1779.
- 21 B. Yu, F. Qi, B. J. Zheng, W. Q. Hou, W. L. Zhang, Y. R. Li and Y. F. Chen, *J. Mater. Chem. A*, 2018, **6**, 1655–1662.
- 22 S. K. Park, J. K. Kim and Y. C. Kang, *Chem. Eng. J.*, 2017, **328**, 546–555.
- 23 X. Q. Wang, J. R. He, B. Yu, B. C. Sun, D. X. Yang, X. J. Zhang, Q. H. Zhang, W. L. Zhang, L. Gu and Y. F. Chen, *Appl. Catal., B*, 2019, **258**, 117996.
- 24 S. Lee, S. Park, J. Park, Y. Kim, K. Yoon, C. Shin, S. Baek, J. Kim, Y.-J. Lee and J. Yi, *Jpn. J. Appl. Phys.*, 2011, **50**, 095801.
- 25 K. Ohmori, N. Esashi, E. K. Atoro, D. K. Sato, H. K. Kawanishi, Y. Higashiguchi and Y. Hayafuji, *Jpn. J. Appl. Phys.*, 2007, **46**, 14–20.
- 26 Y. Hui Fang and Z. P. Liu, *ACS Catal.*, 2014, **4**, 4364–4376.
- 27 Y. M. Shi and B. Zhang, *Chem. Soc. Rev.*, 2016, **45**, 1529–1541.
- 28 D. H. Kweon, M. T. S. Okyay, S. J. Kim, J. P. Jeon, H. J. Noh, N. Park, J. Mahmood and B. J. Beom, *Nat. Commun.*, 2020, **11**, 1278.

